Chemical Analysis and High-Resolution Transmission Electron Microscopy of Porous Silicon with a High-Voltage TEM at 1000 kV

Kazuo Furuya[+], Minghui Song, Yoshio Fukuda, Tetsuji Noda and Tetsuya Saito

National Research Institute for Metals, 3-13 Sakura, Tsukuba, 305 JAPAN
[+]phone: 81-298-59-5053, FAX: 81-298-59-5010, e-mail: furukaz@nrim.go.jp

(Received: Feb. 14, 1997 Accepted: Feb. 21, 1997)

Abstract

The performance of energy dispersive X-ray spectroscopy (HV-EDS) and of energy loss spectroscopy (HV-EELS) for a new analytical high-voltage transmission electron microscope (HVTEM) was described, and their applications were demonstrated for porous silicon (PS), which contains nanocrystals in amorphous substance and shows intense light emission at room temperature. An EDS detector was designed to set in a horizontal position of the HVTEM, and shielding devices of apertures and metal blocks were specially inserted into the column to cut stray X-rays at 1000 kV. A post-column type energy filtered imaging system with additional optical deflection lens for the detector to eliminate stray X-rays was installed below a camera chamber of the HVTEM. High-resolution electron microscopy (HRTEM) revealed Si nanocrystals in the PS layer prepared by an anodization of p-type Si wafer at a current density of 100 mA/cm^2 at room temperature. The chemical analyses of the PS layer indicate the presence of oxygen which is identified from the O-Kα signal with HV-EDS and Si^{4+}-finger print at 108 eV with HV-EELS. Oxygen or oxide related defects at the interface between Si nanocrystals and amorphous are considered to have an important role on the visible light emission from PS layer.

1. Introduction

Analyses of local composition and chemical conditions of materials have been performed using a transmission electron microscope (TEM), having an accelerating voltage less than 200 kV and equipped with energy dispersive X-ray spectroscopy (EDS) and energy loss spectroscopy (EELS). Commercially available field-emission gun (FEG) systems attached to such TEMs are also promoting this trend [1]. A high-voltage TEM (HVTEM) having an accelerating voltage of 1000 kV or more has been considered only for high-resolution transmission electron microscopy [2-3], because of an advantage of the highest point-resolution approaching to 0.1 nm and of a disadvantage of the radiation damage by high-energy electrons. However, the development of advanced materials with atomic arrangements is now requiring the analysis of local composition and chemical conditions, simultaneously with the structural observation.

Attachments of EDS to HVTEM (HV-EDS) had been attempted for AEI-EM7 microscopes in 1980's [4-5]. The preliminary results indicated that the signal to noise ratio in X-ray spectra was low due to the background noise appearing at lower X-ray energies, and that it was not successful to focus a diameter of electron probe less than 1μm. On the other hand, the development of EELS in which a fine focused probe is not required was completed [6], in parallel with the development of second generation of a HVTEM. The new feature of the high-voltage EELS (HV-EELS) is energy filtered imaging, which has become possible to take two dimensional map of selected element by applying a energy window to a EELS spectrum [7]. The first objective of the present paper is to describe a practical performance of HV-EDS and -EELS for a new analytical HVTEM (JEM-ARM1000) developed at National Research Institute for Metals (NRIM). The second objective is to demonstrate the applicability of the HV-EDS and -EELS to an advanced material. The material adopted in this study is porous silicon (PS), which has a visible photoluminescence (PL) about 650 nm at room temperature [8] and is expected to be used for photoelectronic integrated circuits, optical memories, and advanced display systems [9-10]. PS has local compositional changes which is considered due to the oxidation and carbonization in the preparation process as well as an inhomogeneous structure which consists of amorphous and Si nanocrystals. The models proposed for the PL mechanism are so far based on (1) quantum confinement effect in Si nanocrystals [8], (2) surface-confined states at the interface of nanocrystals [11], (3) its related oxide defects [12] and (4) surface chemistry such as siloxene derivatives [13] or SiH_x [14].

The difficulty to determine the PL mechanism lies on the smallness of Si nanocrystals less than 3 nm and on the variation of chemical condition in such small area. The results of HRTEM and chemical analyses of PS layer with HV-EDS and -EELS are presented in the latter section.

2. Experimetal

2.1 High-Voltage EDS and EELS System

JEM-ARM1000 at NRIM has been designed especially for in-situ experiment using heating and cooling holders under electron and ion irradiation. Thus the specimen chamber was fully modified for ion beams and an EDS detector directly facing to a specimen at different angles. A schematic drawing of an outlook of the microscope column is shown in figure 1. Since two ion-introduction ports occupy high angle position, the ultra thin window EDS detector (UTW-EDS) is set in a horizontal position. The modifications made inside of the optical column are to minimize the generation of background X-rays by changing apertures to low-Z materials and to shield the scattered X-rays by heavy metal blocks. Since a LaB_6 thermal emitter was used, the minimum spot size of electron beam is about 10 and 50 nm with a beam current of about 1 nm at 400 and 1000 kV, respectively. A post-column type energy filtered imaging system made of GATAN Ltd. was installed below a camera chamber of the HVTEM. The addition of the optical deflection lens for the detection system to eliminate stray X-rays makes it possible to take HV-EELS spectra and energy filtered TEM (EFTEM) at 1000 kV.

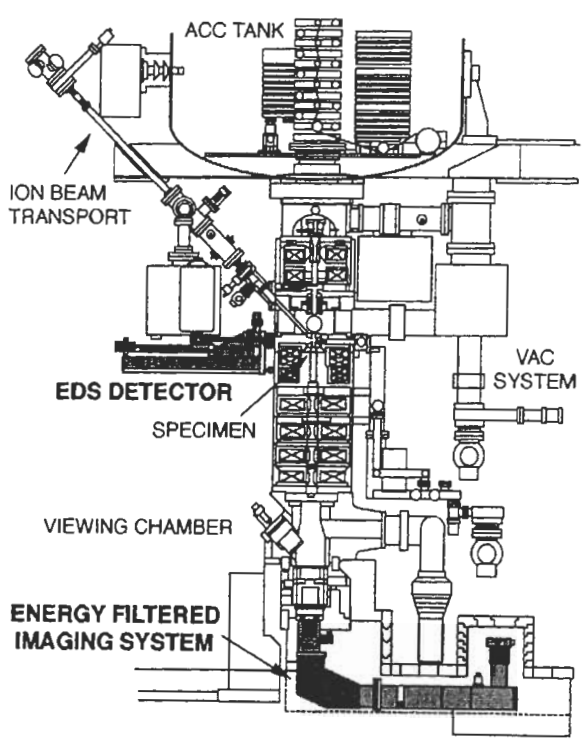

Fig. 1 A shematic drawing of an energy dispersive X-ray spectroscope (HV-EDS) and an energy filtered imaging system (HV-EELS), attached to a newly developed analytical high-voltage transmission electron mictroscope (HVTEM) at NRIM.

2.2 Materials

PS samples were prepared by anodizing boron doped p-type Si (100) wafers with resistivity of 0.04-0.06 Ω.cm. The anodization was performed in the solution of 50wt% HF + C_2H_5OH (1:1) for 10 s. at room temperature at a constant current density of 100 mA/cm^2. As-anodized samples are examined by a PL-lifetime measurement system using a combination of nitrogen laser (wavelength: 337nm, pulse width: 0.3ns) and a streak camera (Hamamatsu C4780). The samples were then made into cross-sectional TEM specimens through a standard argon ion milling method. HRTEM was conducted along the thickness direction of PS layer and the variation of the structure was observed as a function of the distance from surface. HV-EDS and -EELS at 1000 kV were carried out at the same areas where HRTEM was done. The probe current and size of HV-EDS were about 1 nA and 80 nm, respectively. HV-EELS spectra were obtained for Si $L_{2,3}$-edge and O K-edge with the detection area of about 10 nm in diameter and followed by EFTEM in the same region.

3. Results and Discussion

3.1 Performance of HV-EDS and -EELS

The characteristic X-ray spectra of HV-EDS were firstly taken from a type-316 austenitic stainless steel (316 SS) TEM specimen at different accelerating voltages (E) where the electron probe current and diameter were kept constant at 1 nA and about 200 nm, respectively. The 316 SS was chosen for the detection of Cr, Fe and Ni which generate X-rays in the intermediate-energy range in the spectrum. The signal to noise ratios (P/B ratios) obtained from the spectra for Fe-Kα and Ni-Kα are shown in Figure 2 as a function of E, together with the values of a dead time (D) and an energy resolution of the detector (ER). The width of energy window for the peaks and backgrounds was set as 0.2 keV. Since 316 SS

contains about 68 % and 12 % of Fe and Ni, respectively, the P/B ratios are normalized to 100 % values and also shown in the figure. There is little difference between the normalized values for Fe-Kα and those for Ni-Kα. The increase in P/B ratio with increasing E from 400 to 600 kV indicates the improvement of the detection efficiency at higher voltage as reported previously [15-16]. The normalized P/B ratios of both Fe-Kα and Ni-Kα monotonously decreased with further increase in E, nevertheless the ratios kept 105 at 1000 kV. This value is about fifty times larger than those in the previous study [4].

The relative low P/B ratios at 1000 kV was attributed to the increase in the background levels. Uncollimated X-rays along with high energy electrons increased with E, thus the dead time of the detector also increased. However, the energy resolution of the detector showed little increase with increasing E from 142 eV at 400 kV to 159 eV at 1000 kV, where few technical problem remains for the operation of the present EDS system at higher voltages. In addition, it is important to note an advantage of HV-EDS, reported by Furuya et al. [17]. On the contrary to the increase in background levels, the build-up of C-Kα and O-Kα signals during EDS measurement was suppressed at 1000 kV as compared with that at 400 kV, which indicated low contamination rate at higher voltages even in a vacuum less than $2x10^{-6}$ Pa. This is useful to analyze carbon and oxygen containing materials such as PS, because the low concentration of light elements in samples sometimes requires long measuring time and the contamination makes it difficult to perform EDS analyses.

On the HV-EELS, it is important to evaluate the energy resolution attained in a spectrum, because the energy shift due to the change in chemical states is within several eV for most of materials and the P/B ratios of EELS are usually lower than that of EDS. Figure 3 shows two zero-loss spectra obtained from the HV-EELS system operated at 1000 kV with unsaturated and saturated filaments. The full width at half maximum (FWHM) of the zero-loss peak is minimized to be 0.7 eV for unsaturated filament and increases to 1.5 eV for saturated filament. This tendency exhibits that the energy resolution of the system is not controlled by the thermal drift of photodiode detector, but by the temperature change of the LaB_6 thermal emission filament. One should point out that the meaningful resolution of the HV-EELS is 1.5 eV, even if finer structures can be observed in a spectrum.

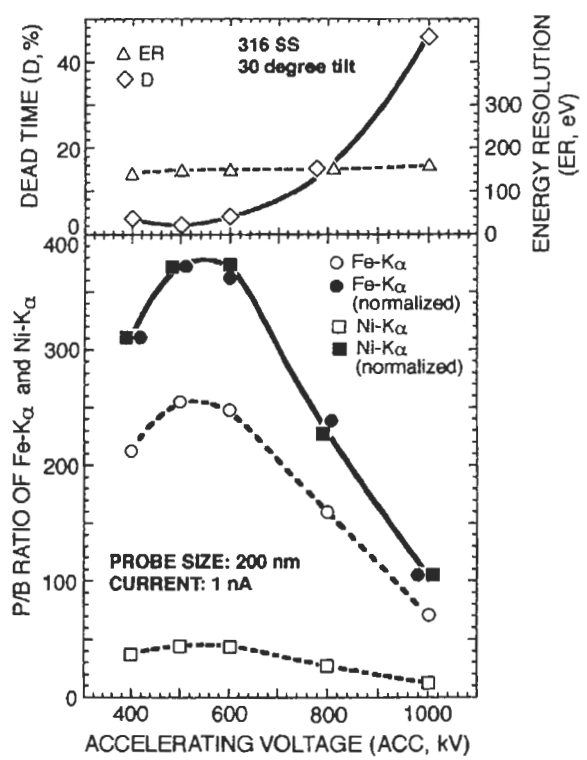

Fig. 2 The signal to noise (P/B) ratio of Fe-Kα and Ni-Kα , dead time (D) and energy resolution (ER) in the HV-EDS measurements as a function of an accelerating voltage (E).

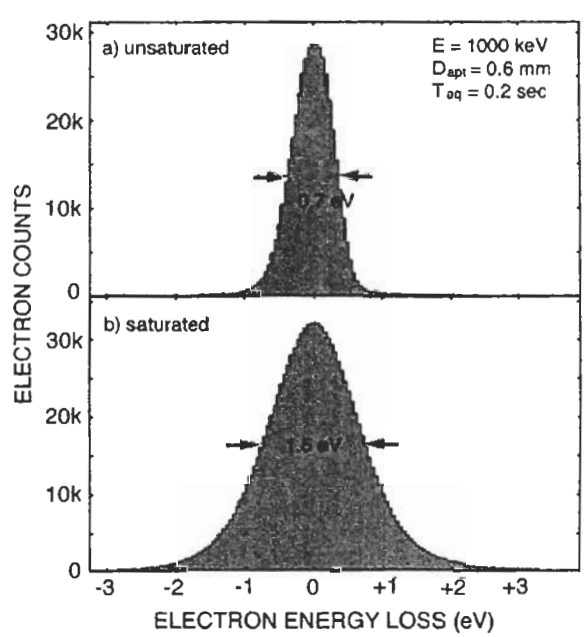

Fig. 3 Zero-loss spectra obtained form the HV-EELS system, showing the resolution of 0.7 and 1.5 eV with unsaturated and saturated filament, respectively.

3.2 Structure and Chemical Conditions of Porous Silicon

Prior to performing HV-EDS and -EELS with HRTEM, the intense PL from the PS layer was confirmed to have a peak wavelength of about 640 nm. The broadness of PL spectrum and the multi-exponential decay of PL implied several mechanisms concerning with the visible light emission from PS layer. The cross sectional TEM images of PS layer along [110] direction are shown in Figure 4 with changing the positions from the surface. A low magnification photograph (Fig.4-a)) indicates microscopic inhomogeneity depending on the distance from surface. The near surface region consists of a sponge-like structure which has 150 to 200 nm of thickness and has no clear diffraction contrast. However, a HRTEM image (Fig.4-b)) reveals small nanocrystals of 2 to 3 nm in diameter embedded in amorphous substance. The shape of the nanocrystals are not clear, because Si nanocrystals are reported to become unstable when the size is less than about 3 nm [18]. Also such a nanocrystal may be chemically influenced by fluorine during anodization and by carbon contamination during the specimen preparation process for TEM.

The tree-like structure is observed to develop on the sponge-like structure, so that the interface between PS layer and Si substrate becomes zigzag. The pattern at the interface does not have a particular crystallographic orientation relationship. The size distribution and mean size of nanocrystals become large with increasing the distance from surface. The size of crystals at the middle of the PS layer becomes more than 10 nm, which exceeds the limit of the particle size for visible light emission due to the quantum confinement effects [19].

Figure 5 exhibits the results of HV-EDS analysis of porous silicon (PS) at 1000 kV, taken at corresponding points of A_{EDS} to C_{EDS} in Fig. 4. The background X-ray spectrum was also shown together in Fig. 5-a) and -b), because of its measurable level at 1000 kV. It should be noted that a considerable amount of oxygen and carbon presents in PS layer. The intensity of O-Kα does not change when the distance from surface increases, while that of C-Kα decreases. Canham et al. [20] have already reported blue light emission due to the carbon contamination of PS which exposed in air for several months. Although the exposure of PS specimens in air was limited within several days for the present study, the

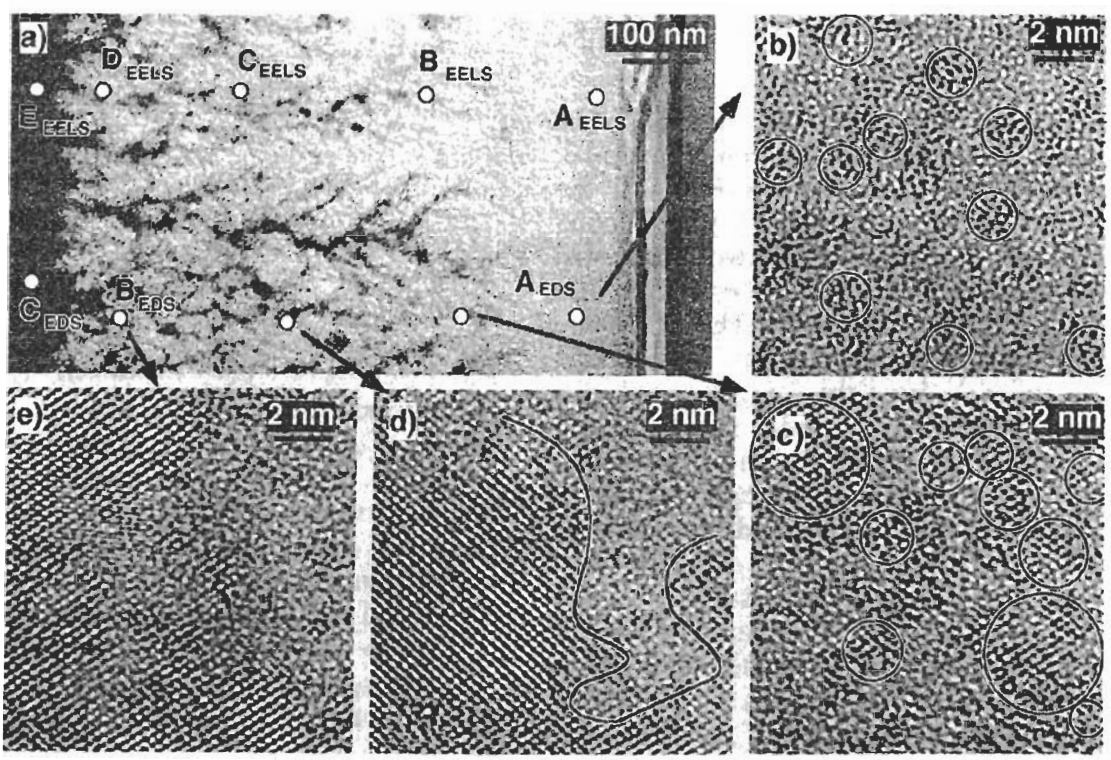

Fig. 4 Cross sectional transmission electron microscopy of porous silicon (PS) anodized in HF solution at a current density of 100 mA/cm^2 for 10 s at room temperature. a) low magnification photograph, b) to e) corresponding HRTEM images with changing the distance from surface.

contamination of PS surface by carbon was not eliminated in the course of the preparation.
HV-EELS analysis at 1000 kV were carried out at different positions of PS layer, shown as A_{EELS} to E_{EELS} in Fig. 4 and the results are presented in Figure 6. Si $L_{2,3}$-edge and O K-edge are chosen among other edges because of

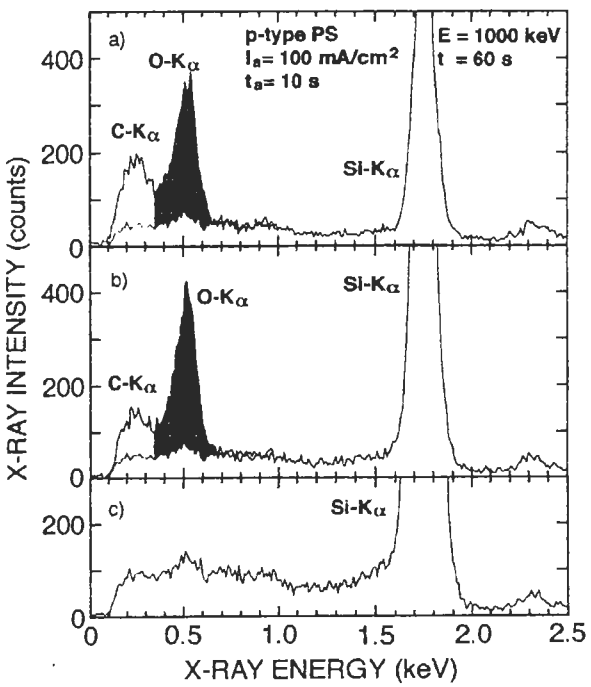

Fig. 5 The results of HV-EDS analysis of porous silicon (PS) at 1000 kV for 60 s. a) to c) correspond to the spectra taken at A_{EDS} to C_{EDS} in Fig. 4.

the sensitivity to chemical bonds. The background was subtracted assuming the power law of energy loss curves. In Fig.6-a), the energy loss near edge structures (ELNES) of Si $L_{2,3}$-edge are presented with two concerned peaks noted as Si^{0+} (the energy loss ΔE = 100 eV) and Si^{4+} (ΔE = 108 eV). The Si^{0+} edge originates from 4-fold Si atoms in diamond structure and Si^{4+} from the "finger-print" of a Si-4O tetrahedron. The Si^{4+} edge is always seen in the spectra of PS layer, and its relative intensity becomes stronger as approaching to the surface. On the other hand, the relative intensity of Si^{0+} edge rapidly decrease with decreasing the distance from surface. Small amount of Si^{2+} (ΔE = 103 eV) can be observed in intermediate region. Schuppler et al. [21] have reported NEXAFS spectra of PS layers and indicated the decrease in Si^{4+} signal and the increase in Si^{2+} (ΔE = 103 eV) signal as increasing the particle size of PS. The similar behavior is observed that small amount of Si^{2+} can be found in intermediate region. Corresponding O K-edge shows consistent tendency, namely large amount of oxygen detected near surface region. Small amount of O K-edge signal from Si substrate comes from the slightly oxidized specimen surface or oxygen injected into Si substrate during

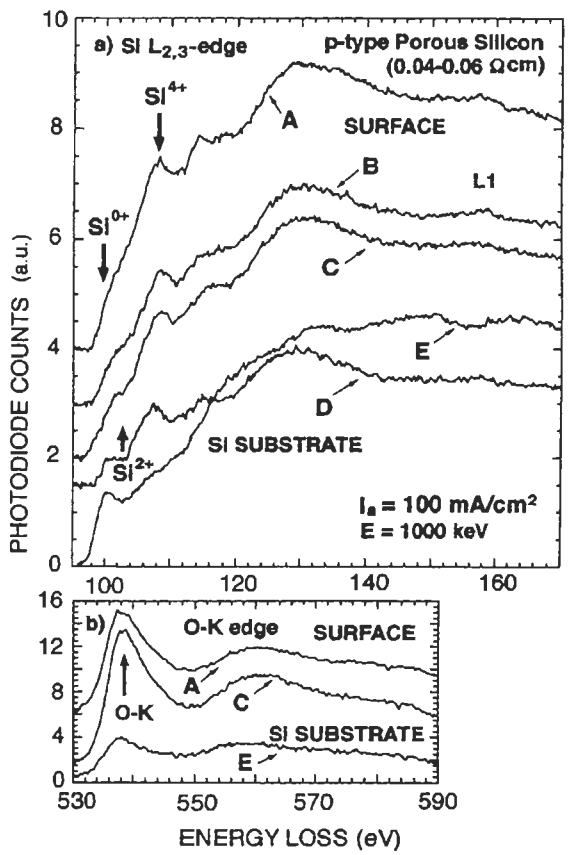

Fig. 6 The results of HV-EELS analysis of porous silicon (PS) at 1000 kV. a) Si L2,3-edge and b) O K-edge. A to E correspond to the spectra taken at A_{EELS} to E_{EELS} in Fig. 4.

anodization.
The spatial distribution of oxygen and silicon in PS layer is a key factor to control the mechanism of PL and is evaluated with energy filtered transmission electron microscopy (EFTEM). EFTEM was carried out at the boundary region between sponge- and tree-like structures and for Si $L_{2,3}$-edge and O K-edge with an energy window of 20 eV. A zero-loss image and elemental maps for Si $L_{2,3}$-edge and O K-edge are shown in Figure 7. Comparing with the zero-loss image, clearly indicated is a good agreement between the morphology and chemical maps. The Si structure does not provide an uniform shape of crystals and sometime remains as a skeleton or withered

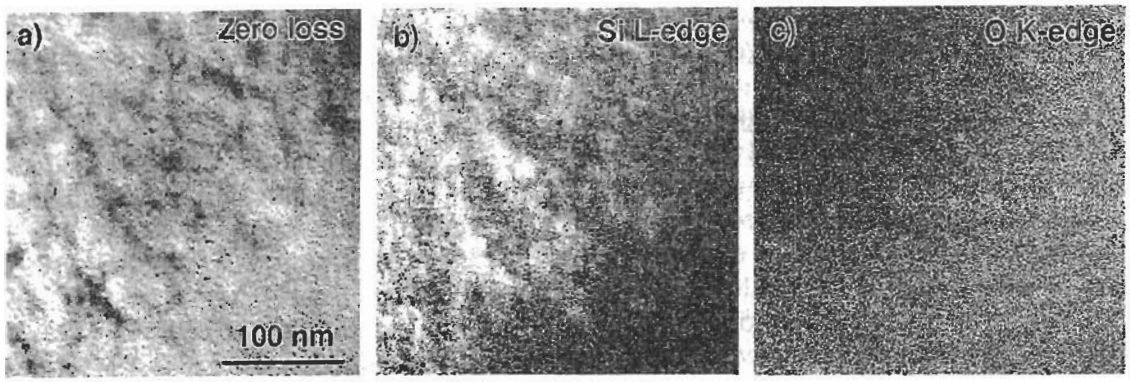

Fig. 7 Energy filtered TEM images of porous silicon (PS) at 1000 kV, taken near the boundary region between sponge and tree-like structures in Fig. 4. The energy window is 20 eV. a) a zero-loss image by elasically scattered electrons, b) an elemental map by Si $L_{2,3}$-edge and c) that by O K-edge.

twig. The content of Si is larger in the tree-like structure, while that of O is larger in the sponge-like structure. Due to the resolution of EFTEM in Fig. 7, it is not successful to evaluate the distribution of oxygen around individual nanocrystals. But the figure reveals that the content of oxygen increases with decreasing the size of nanocrystals less than 3 nm in sponge-like structure region.

The present results demonstrate that the importance of the local chemical conditions of PS layer, especially the existence of oxygen in Si-complex, as well as the heterostructures contains Si nanocrystals. The PL has been reported from bulk SiO_2 [22] and impurities [20], and these turns out to be not responsible for the visible PL from the PS layer. Therefore, the quantum confinement effect and defects in Si-O complex in conjunction with Si nanocrystals can be an important candidate for the origin of the PL.

The light emission due to quantum confinement effects in nanocrystals has been investigated for Si or Ge implanted SiO_2 [23-24]. The size of nanocrystals was controlled by the annealing at different temperature and showed a narrow Gaussian distribution in most cases. Clearly reported was a peak wavelength shift from red to blue region as decreasing the mean size of nanocrystals. Since the size distribution of nanocrystals in the present PS layer depended on the distance from surface, clear correspondence of the PL and particle size could not be obtained due to complicated Si and Si-O structures. But it should be pointed out that unclear images of nanocrystals in Fig. 4 implies the inperfectness of crystallographic structures inside and outside the particles. Therefore, the strain might have effects on the quantum confinement effects in nanocrystals.

The presence of oxygen in PS layer has been reported [25] and was discussed in terms of PL associated with dangling bonds in Si-O bonds. But the same intensity of O-Kα in Fig. 5 with changing structure from sponge-like (fine nanocrystals) to tree-like (large crystals) implies further complicated mechanisms with defects. One of possible defects is the non-bridging oxygen hole center (NBOHC) [26-27], which consists of a Si vacancy in SiO_2 tetrahedron-structure and has a PL peak at 1.85-1.9 eV (wavelength from 670 to 652nm) and a PL life time of 10-15μs. Since PS layers have been oxidized at room temperature in the pressures of oxygen as low as 1×10^{-5} torr [28], the oxidation takes place at the interface and the surface between amorphous (SiO_2) and Si nanocrystals. This process is equivalent to the migration of Si^{4+} ions and electrons to outer oxide (amorphous) region. The tendency of the distributions of Si^{4+} in Fig. 6 and of oxygen in Fig.7 supports the formation of the considerable amount of NBOHC in the PS layer. Although the local distribution of NBOHC and nanocrystals could not be determined in the present study, the present results indicate an importance of the interaction between Si-O bond states with defects and Si-nanostucture for PL from PS layers.

4. Conclusions

An energy dispersive X-ray spectroscope (HV-EDS) and an energy loss spectroscope (HV-EELS) were developed for a new analytical high-voltage transmission electron microscope (HVTEM) at National Research Institute for Metals (NRIM), and their applications were demonstrated for porous silicon (PS), which

contains Si nanocrystals in amorphous substance and shows intense light emission at room temperature.

(1) An EDS detector was designed to set in a horizontal position of the HVTEM, and the shielding devices of apertures and metal blocks made it possible to measure characteristic X-ray spectra at 1000 kV. A post-column type energy filtered imaging system was installed below a camera chamber of the HVTEM, with additional optical deflection lens for the detector to eliminate stray X-rays.

(2) High resolution electron microscopy (HRTEM) revealed Si nanocrystals in PS layer prepared by an anodization of p-type Si (100) wafer at a current density of 100 mA/cm^2 at room temperature. The chemical analysis of the PS layer indicated the presence of oxygen which is identified from the O-Kα signal in HV-EDS spectra and Si^{4+}-finger print at 108 eV with HV-EELS spectra.

(3) Oxygen or oxide related defects at the interface between Si nanocrystals and amorphous are considered to have an important role on the visible light emission from PS layer.

References

1. T. Honda, T. Tomita, T. Kaneyama, and Y. Ishida, Ultramicroscopy, **54**, 132 (1994)
2. F. Phillipp, R. Höschen, M. Osaki, G. Möbus and M. Rühle, Ultramicroscopy, 56, 1 (1994)
3. Y. Matsui, S. Horiuchi, Y. Bando, Y. Kitami, M. Yokoyama, I. Matsui and T. Katsuta, Ultramicroscopy, **39**, 8 (1991)
4. F. G. Beckitt, D. J. Dyson, T. Glacman and D. T. Llewellyn, Scheffield Laboratories Report, SH/PROD/PM/6721/4/81/B (1981)
5. W. F. Tivol, D. Barnard, T. Guha, in Proc. 7th Intern. Conf. High-volt. Electron. Microsc., Berkeley, 1983, p129
6. O. L. Krivanek, A. J. Gubbens, N. Dellby and C. E. Meyer, Microscopy Microanal. Microstruct., 3, 187 (1992)
7. A. J. Gubbens, B. Kraus, O. L. Krivanek and P. E. Mooney, Ultramicroscopy, **59**, 255 (1995)
8. L. T. Canham, Appl. Phys. Lett., **57**, 1046 (1990)
9. P. Steiner, F. Kozlowski and W. Lang, Appl. Phys. Lett., **62**, 2700 (1993)
10. C. Tsai, K. -H. Li, J. C. Cambell and A. Tasch, Appl. Phys. Lett., **62**, 2818 (1993)
11. F. Koch and V. Petrova-Koch, in Porous Silicon, edited by Z. C. Feng and R. Tsr (World Scientific, Singapore, 1994), p.133
12. G. C. Qin and Y. Q. Jia, Solid State Comun., **86**, 559 (1993)
13. M. S. Brandt, H. D. Fuchs, M. Struzmann, J. Weber, and M. Cardona, Solid State Commun., **81**, 307 (1992).
14. C. Tsai, K. -H. Li, D. S. Kinosky, R. -Z. Wian, T. -C. Hsr, J. t. Irby, W. K. Banerjee, A. F. Tasch, J. C. Campbell, B. K. Hance, and J. M. White, Appl. Phys. Lett., **60**, 1700 (1992)
15. Y. Bando, Y. Matsui, Y. Kitami, Y. Inomata, Y. Honda and Y. Harada, Jpn. J. Appl. Phys., **23**, L412 (1984)
16. S. Suzuki and H. Kitajima, J. Electron Microsc., **35**, 335-342 (1986)
17. K. Furuya, M. Osaki, M. Awaji and T. Saito, J. Electron Microsc., **45**, 285 (1996)
18. S. Veprek, Z. Iqbal and F. -A. Sarott, Phil. Mag., **B45**, 137 (198)
19. T. Takagahara and K. Takeda, Phys. Rev., **B46**, 15578 (1992)
20. L. T. Canham, A. Loni, P. D. J. Calcott, A. J. Simons, C. Reeves, M. R. Houlton, J. P. Newey, K. J. Nash and T. I. Cox, Thin Solid Films, **276**, 112 (1996)
21. S. Schuppler, S. L. Friedman, M. A. Marcus, D. L. Adler, Y. -H. Xie, F. M. Ross, Y. J. Chabal, T. D. Haris, L. E. Brus, W. L. Brown, E. E. Chaban, P. F. Szajowski, S. B. Christman and P. H. Citrin, Phys. Rev. B, **52**, 4910 (1995)
22. J. H. Stahis and M. A. Kastner, Phys. Rev., **B35**, 2972 (1987)
23. C. M. Yang, K. V. Shcheglov, K. J. Vahala and H. A. Atwater, Nucl. Instr. Methods Phys. Res., **B106**, 433 (1995)
24. K. S. Min, K. V. Shcheglov, C. M. Yang, H. A. Atwater, M. L. Brongersma and A. Polman, Appl. Phys. Lett., **69**, 2033 (1996)
25. D. W. Cooke, B. L. Bennett, E. H. Farnum, W. L. Hults, K. E. Sickafus, J. F. Smith, J. L. Smith, T. N. Taylor, P. Tiwari and A. M. Portis, Appl. Phys. Lett., **68**, 1663 (1996)
26. A. Anedda, G. Bongiovanni, M. Cannas, F. Congiu, A. Mura and M. Martini, J. Appl. Phys., **74**, 6993 (1993)
27. S. M. Prokes and W. E. Carlos, J. Appl. Phys., **78**, 2671 (1995)
28. P. Gupta, V. L. Covlin and S. M. George, Phys. Rev., **B37**, 8234 (1988)